2017 American Control Conference
Sheraton Seattle Hotel
May 24–26, 2017, Seattle, USA

Development and Experimental Validation of a Dual Extended Kalman Filter for Three Way Catalytic Converter

Simone Gelmini[1], Stefano Sabatini[2], Mark A. Hoffman[1] and Simona Onori[1,*]

***Abstract*— A three way catalytic converter (TWC) is responsible for conversion of engine out hazardous pollutants such as carbon monoxide (CO), nitrogen oxides (NO_x) and hydrocarbons (HC) into carbon dioxide (CO_2), water (H_2O) and (N_2) nitrogen. TWC conversion efficiency highly depends on the amount of oxygen stored in the converter, or State of Oxygen (SOX). Estimation of SOX during real time operation is key controlling the TWC behaviour maximizing its efficiency. Moreover, the decrease of TWC conversion efficiency over converter lifetime due to mechanical, chemical and thermal factors, is observed through the decrease of a macroscopic quantity, the Oxygen Storage Capacity (OSC). In this paper, a Dual Extended Kalman Filter (d-EKF) to estimate TWC SOX and OSC is presented. The observer is built upon an experimentally validated, physics-based model of the converter developed by the same authors in a previous work. The nonlinear partial differential equation-based TWC model is properly adapted, through the finite discrete method, for real-time estimation within a vehicle engine-control unit (ECU). Experimental results collected from a TWC instrumented with wide-range oxygen sensors show the ability of the dual observer to robustly estimate both SOX and the catalyst age.**

NOMENCLATURE

λ	Normalized air fuel ratio	
t	Time	$[s]$
z	Axial dimension	$[m]$
ρ_g	Exhaust gas density	$\left[\frac{kg}{m^3}\right]$
ϵ	TWC open cross sectional area	$[0-1]$
c_{p_g}	Specific heat of the exhaust gas	$\left[\frac{J}{kg\cdot K}\right]$
T_g	Gas temperature	$[K]$
$\dot{m}_{exh}$	Exhaust gas mass flow rate	$\left[\frac{kg}{s}\right]$
A_{cs}	TWC cross sectional area	$[m^2]$
h	Convective heat transfer coefficient	$\left[\frac{W}{m^2\cdot K}\right]$
A_{geo}	TWC specific geometric area	$\left[\frac{m^2}{m^3}\right]$
T_{cat}	TWC solid phase temperature	$[K]$
T_{cat_0}	TWC solid phase temperature at the initial time ($t=0$)	$[K]$
T_{exh}	Exhaust gas temperature	$[K]$
ρ_s	TWC solid phase density	$\left[\frac{kg}{m^3}\right]$
c_{p_s}	TWC solid phase specific heat	$\left[\frac{J}{kg\cdot K}\right]$
λ_s	TWC solid phase conductivity	$\left[\frac{W}{m\cdot K}\right]$
A_{out}	TWC external surface	$[m^2]$
V_{cat}	TWC volume	$[m^3]$
h_{out}	Convective heat transfer coefficient with the environment	$\left[\frac{W}{m^2\cdot K}\right]$
T_{amb}	Ambient temperature	$[K]$
ΔH_l	Reaction enthalpy difference for the l^{th} reaction	$\left[\frac{J}{mol}\right]$
R_l	Reaction rate for the l^{th} reaction	$\left[\frac{mol}{m^3\cdot s}\right]$
K_{reac}	Proportional constant of $\dot{Q}_{reac}$	$\left[\frac{J}{kg\cdot m^3}\right]$
η	TWC efficiency function	
c_0	Total exhaust gas concentration	$\left[\frac{mol}{m^3}\right]$
k_j^f	Forward reaction rate ($j=1,2$)	
k_j^b	Backward reaction rate ($j=1,2$)	
P	Exhaust gas pressure	$[Pa]$
R	Universal gas constant ($R=8.314$)	$\left[\frac{J}{kg\cdot K}\right]$
A_j	Arrhenius pre-exponential factor	
E_j	Activation energy ($j=1,2$)	$[J]$
K_j	Chemical equilibrium constant	
u	Space velocity	$\left[\frac{m}{s}\right]$
M_{exh}	Average molar mass of exhaust gas composition	$\left[\frac{kg}{mol}\right]$
OSC	Oxygen storage capacity	$\left[\frac{mol}{m^3}\right]$
SOX	State of Oxygen	$[0-1]$
Δz	Spatial discretization length	$[m]$
$\mathcal{N}(\mu,\sigma^2)$	Gaussian white noise of mean μ and variance σ^2	

NOTATION

j	Reactions index
k	Discrete time index
i	Discrete cell index
c	Chemical species index

I. INTRODUCTION

Environmental concerns have led to stricter emission regulations on passenger vehicles over the past years [1]. Aftertreatment technologies such as catalytic converters, particulate filters and exhaust gas recirculation systems have been adopted by automakers as valuable solutions to comply with emission regulations. The increasing complexity of the new exhaust emission systems requires sophisticated tools for on-board control and diagnostics. The adoption of physics-based models in conjunction with optimization-based control techniques is currently being the trend pursued by the automotive industry to tackle these pressing issues.

[1]Department of Automotive Engineering, International Center for Automotive Research, Clemson University, Greenville, South Carolina 29607 {sgelmin,mhoffm4,sonori}@clemson.edu

[2]Dipartimento di Elettronica, Informazione e Bioingegneria - Politecnico di Milano, via Ponzio 34/5 20133 Milano, Italy stefano.sabatini90@gmail.com. Stefano was a visiting scholar at CU-ICAR at the time of this work

[*] corresponding author

The TWC simultaneously converts engine emitted toxic exhaust gases by catalysing a redox reaction. Carbon monoxide CO, hydrocarbons HC and nitrogen oxides NO_x are converted into nitrogen N_2, carbon dioxide CO_2 and water H_2O with a conversion efficiency higher than 99% [2] when working near stoichiometry and at temperature higher than catalyst light-off temperature [3].

During real driving conditions, transient variations of the air/fuel ratio affect the TWC conversion efficiency. Significant performance improvements are obtained by incorporating base metal promoters such as cerium (Ce) in the TWC washcoat. Cerium significantly enhances NO_x and CO conversion performance near stoichiometry, and increases TWC durability against thermal deterioration.

The control of the oxygen stored level, SOX, enables simultaneous oxidation and reduction of exhaust species by ensuring that the TWC is neither saturated nor devoided of oxygen. The ability to effectively model the oxygen storage dynamics allows the on-board controller to robustly regulate the air/fuel ratio, so to improve TWC efficiency during driving operation. However, the total oxygen storage capacity, OSC, of the TWC degrades with age due to both thermal and chemical phenomena. Thus, accurate control of SOX depends directly on accurate and age dependent estimation of OSC.

The goal of this paper is to present the design of a model-based estimation scheme, for oxygen storage dynamics and oxygen storage capacity, using a dual-Kalman filter approach. TWC oxygen storage observers proposed in the literature are based on semi-empirical models owing to their computational efficiency. The work proposed in [4] utilizes a recursive Markov method to adapt the model parameters online, using upstream and downstream lambda oxygen sensors, without any consideration of aging effects. In [5], the oxygen storage rate is monitored by a switched linear observer with multiple Lyapunov functions, designed by solving several linear matrix inequalities, while the value of OSC is estimated with recursive least squares. In [6] a non-linear least squares problem is formulated based on a moving horizon estimation strategy. In a recent work [7], Support Vector Machines (SVM) method is used with a simple TWC dynamical model to design a TWC diagnostics monitoring algorithm, capable of separating out differently aged catalysts.

In [8], an Extended Kalman Filter (EKF) is proposed for estimating both SOX and OSC using a switch-type lambda sensor downstream the catalyst. However, in this work the amount of oxygen stored estimated by the EKF is only related to the last discretization cell and not for the entire catalyst owing to observability issues on the first cells. In [9], an adaptive backstepping control approach is used to design an EKF to estimate OSC and exhaust gas temperature dynamics, leading to a 22 state-model.

In this paper, a dual Extended Kalman Filter (d-EKF) is developed that simultaneously estimates SOX and OSC. The dual observer scheme is developed using the control-oriented model derived from the physics-based model previously designed by the authors [10], [11] and wide-band lambda sensors, placed upstream and downstream the catalyst, respectively.

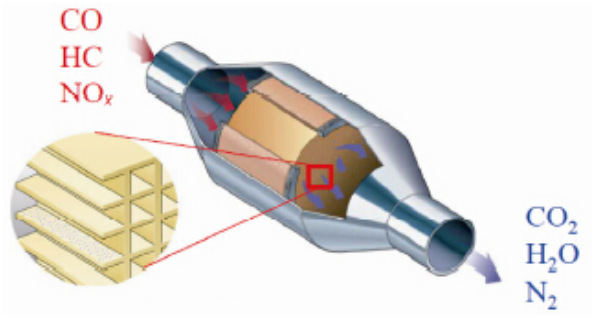

Fig. 1: TWC cutaway showing the internal honeycomb structure of the converter [12].

The paper is organized as follows. In Section II, the TWC model and the experimental set-up are described. The derivation of the control oriented model is presented in Section III, and used in Section IV and Section V, to design, simulate and calibrate the d-EKF. Final remarks are outlined in Section VI.

II. TWC Experimental layout

The TWC is a passive gas exhaust aftertreatment device composed of a substrate, a wash-coat and a mix of precious metals. The substrate is generally a honeycomb ceramic monolith through which the exhaust gas flows. A washcoat is applied to the substrate, providing a porous layer on which the catalytic materials, in the form of a mixture of Platinum, Palladium and Rhodium - are placed to enable the conversion of pollutants (see, Fig. 1). Cerium is also added to enhance the storage capability of the converter.

In this work, experimental data have been acquired over an aged catalyst, referred to as OBD cat. This aged catalyst underwent an aging procedure to represent a catalyst that is degraded well beyond the full useful life emissions standard ($> 150,000$ miles). Detailed about the aged catalyst are found in [13]. The geometric properties of the TWC tested in the lab are listed in Table I.

	Brick
Length [mm]	68
Volume [l]	0.597
Precius metal loading [g/l]	0-2.2-0.15

TABLE I: Catalyst specifications.

The converter was instrumented with two wide-band lambda sensors - λ_{pre} upstream and λ_{mid} downstream - and two thermocouples - one to measure the inlet exhaust gas temperature, T_{exh}, and the second to measure the internal TWC temperature, T_{cat} [13]. The exhaust mass flow rate $\dot{m}_{exh}$ was recorded on the ECU. The sensor layout is shown in Figure 2.

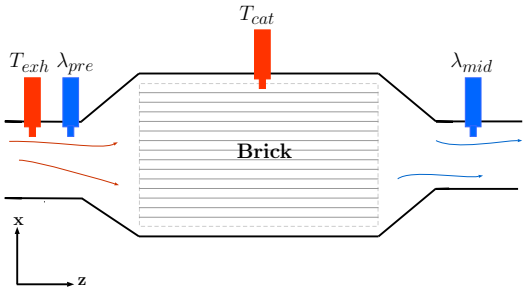

Fig. 2: An overview of the schematic TWC and of the sensor layout used in the experiment conducted in this work: in red the thermocouples at the inlet and in the catalyst location; in blue the wide band lambda sensors in the pre and mid location.

III. TWC PHYSICS BASED MODEL

The TWC physics-based model used for the d-EKF design captures both the thermal and oxygen storage dynamics. The thermal model takes into account the temperature variation in both the exhaust gas and the TWC substrate. The oxygen storage model coupled with the thermal dynamics, predicts the amount of oxygen stored in the catalyst by means of the adsorption and desorption mechanisms due to the deviations of the air/fuel ratio from the stoichiometry.

A. Thermal model

Using a similar approach to the one proposed in [14], the thermal model is composed of two nonlinear PDEs describing the energy balance of the gas and the solid phase.

Energy balance of the gas phase: The energy balance of the gas phase models the heat exchanged with the solid phase and the heat diffusion in the gas phase along the flow axis z.

$$\rho_g \cdot \epsilon \cdot c_{p_g} \cdot \frac{\partial T_g}{\partial t} = -\frac{\dot{m}_{exh}}{A_{cs}} \cdot c_{p_g} \cdot \frac{\partial T_g}{\partial z} + h \cdot A_{geo} \cdot (T_{cat} - T_g) \quad (1)$$

where $-\frac{\dot{m}_{exh}}{A_{cs}} \cdot c_{p_g} \cdot \frac{\partial T_g}{\partial z}$ is the heat of the exhaust gas flowing along the TWC flow axis and $h \cdot A_{geo} \cdot (T_{cat} - T_g)$ is the heat exchanged between the gas and the catalyst. Owing to gas temperature dynamics being faster than catalyst temperature, the storage term $\rho_g \cdot \epsilon \cdot c_{p_g} \cdot \frac{\partial T_g}{\partial t}$ in (1) is neglected, thus considering steady state values for T_g, leading to the boundary condition:

$$T_g(t, z = 0) = T_{exh}(t) \quad (2)$$

where the initial (spatial) conduction of the gas, is assumed to be equal to the measured exhaust gas temperature T_{exh}.

Energy balance of the solid phase: The energy balance equation of the solid phase describes the storage and the conduction inside the catalyst substrate, the convection with the gas phase and with the environment and the heat released during the chemical reactions according to the following equation:

$$\rho_s \cdot (1-\epsilon) \cdot c_{p_s} \cdot \frac{\partial T_{cat}}{\partial t} = (1-\epsilon) \cdot \lambda_s \cdot \frac{\partial^2 T_{cat}}{\partial z^2} + \sum_l (-\Delta H_l \cdot R_l) - h \cdot A_{geo} \cdot (T_{cat} - T_g) - h_{out} \cdot \frac{A_{out}}{V_{cat}} \cdot (T_{cat} - T_{amb}) \quad (3)$$

where $(1-\epsilon) \cdot \lambda_s \cdot \frac{\partial^2 T_{cat}}{\partial z^2}$ and $h \cdot A_{geo} \cdot (T_{cat} - T_g)$ take into account the conduction and the convection between gas and substrate, respectively. Heat loss to the ambient is accounted for by $h_{out} \cdot \frac{A_{out}}{V_{cat}} \cdot (T_{cat} - T_{amb})$, whereas $\sum_l (-\Delta H_l \cdot R_l)$ represents the heat released during the exothermic reactions. As in [15], conduction along the substrate can be neglected due to low conductivity of the cordierite substrate. The term $\sum_l (-\Delta H_l \cdot R_l)$ representing the heat released during exothermic reactions and indicated with $\dot{Q}_{reac}$ and is assumed to be proportional to the exhaust mass flow rate $\dot{m}_{exh}$ as follows:

$$\dot{Q}_{reac} = K_{reac} \cdot \dot{m}_{exh} \cdot \eta(T_{cat}) \quad (4)$$

where $\eta(T_{cat})$ is a S-shaped efficiency function [3]. Assuming negligible conduction, the initial condition of (3) is the temperature along the flow axis at the initial time instant:

$$T_{cat}(t = 0, z) = T_{cat_0}(z) \quad (5)$$

B. Oxygen storage model

To improve TWC performance, cerium is added that function as an oxygen buffer either storing or releasing oxygen when needed during transients. The main chemical reactions for the oxygen storage and release are given by [16]:

$$O_2 + 2 \cdot Ce_2O_3 \longleftrightarrow 2 \cdot Ce_2O_4 \quad (6a)$$

$$CO + Ce_2O_4 \longleftrightarrow CO_2 + Ce_2O_3 \quad (6b)$$

where Ce_2O_3 is the reduced cerium oxide concentration, while Ce_2O_4 is the oxidized cerium oxide concentration. The first reaction (6a) accounts for the oxygen adsorption on the catalyst surface whereas the second (6b) considers the CO oxidation with the oxygen already adsorbed.

$$R_1 = k_1^f \cdot [Ce_2O_3]^2 \cdot [O_2] - k_1^b \cdot [Ce_2O_4]^2 \cdot c_0 \quad (7a)$$

$$R_2 = k_2^f \cdot [Ce_2O_4] \cdot [CO] - k_2^b \cdot [Ce_2O_3] \cdot [CO_2] \quad (7b)$$

account for both the the forward (f) and backward (b) reactions described in (6a) and (6b). The symbol $[\mathcal{X}]$ is used to indicate the concentration of the chemical species $\mathcal{X}$, in $\left[\frac{mol}{m^3}\right]$, where $\mathcal{X} = O_2,\ CO,\ CO_2,\ Ce_2O_3,\ Ce_2O_4$. The total exhaust gas concentration, c_0, is equal to $c_0 = \frac{P}{R \cdot T_g}$, where the exhaust gas pressure is set to $P = 1 \cdot 10^5\ [Pa]$, [16]. The forward reaction rate k_j^f (with $j = 1, 2$) is a temperature dependent term following the Arrhenius equation. The backward reaction constant k_j^b (with $j = 1, 2$) is evaluated as the ratio between the forward reaction rate and the chemical equilibrium constant K_j. The equilibrium constant is taken as a function of the Gibbs energy difference ΔG_j (with $j = 1, 2$), for the details of this derivation, please refer to [16]. Species concentration dynamics can be described by means of the following set of PDEs, [14]:

$$\begin{aligned} \frac{\partial [O_2]}{\partial t} &= -u \cdot \frac{\partial [O_2]}{\partial z} - R_1 \\ \frac{\partial [CO]}{\partial t} &= -u \cdot \frac{\partial [CO]}{\partial z} - R_2 \\ \frac{\partial [CO_2]}{\partial t} &= -u \cdot \frac{\partial [CO_2]}{\partial z} + R_2 \end{aligned} \quad (8)$$

where u, the space velocity, is approximated as a function of the mass flow rate $\dot{m}_{exh}$:

$$u = \frac{\dot{m}_{exh}}{c_0 \cdot M_{exh} \cdot A_{cs}} \tag{9}$$

Given that the exhaust gas dynamics is much faster than the oxygen storage dynamics, the concentration storage term is neglected, [17]. The OSC is the effective catalyst "capacity" corresponding to the volume of active sites, and defined as the amount of oxidized and empty surface sites in the converter as:

$$[Ce_2O_3] + [Ce_2O_4] = OSC \tag{10}$$

The SOX, also denoted by ϕ, with $0 < \phi < 1$, is the fraction (relative to the total capacity) of oxygen storage sites occupied in the catalyst, whose dynamics are described by, [16]:

$$\frac{\partial \phi}{\partial t} = \frac{1}{OSC} \cdot (2 \cdot R_1 - R_2) \tag{11}$$

A model for the air/fuel ratio is determined from gas concentrations [16]:

$$\lambda = \frac{2 \cdot ([O_2] + [CO_2]) + [CO]}{2 \cdot ([CO] + [CO_2])} \tag{12}$$

Both the temperature and the oxygen models have been identified and validated against experimental data collected at Clemson University International Center for Automotive Research (CU-ICAR) over real driving cycles. For more details, see [10] and [13].

C. Model discretization

In order to design a d-EKF for TWC, the temperature and the oxygen storage models are spatially discretized to remove the spatial dependence. Following [18], the finite discretization method (FDM) has been performed using a finite difference upwind scheme, on which the general spatial derivative $\frac{df(z)}{dz}$ is substituted with $\frac{f^i - f^{i-1}}{\Delta z}$, where superscript i indicates the i^{th} discretization cell and Δz is the spatial discretization step. Eq. (1) is therefore rewritten as

$$T_g^i = \frac{T_g^{i-1} + \frac{h \cdot A_{geo} \cdot A_{cs} \cdot \Delta z}{\dot{m}_{exh} \cdot c_{p_g}} \cdot T_{cat}^i}{1 + \frac{h \cdot A_{geo} \cdot A_{cs} \cdot \Delta z}{\dot{m}_{exh} \cdot c_{p_g}}} \tag{13}$$

with no explicit time dependence, whereas (3) is simplified into a set of Ordinary Differential Equations (ODEs) as follows:

$$\begin{aligned} \frac{dT_{cat}^i}{dt} &= -\frac{h \cdot A_{geo}}{\rho_s \cdot (1-\epsilon) \cdot c_s} \cdot \left(T_{cat}^i - T_g^i\right) \\ &+ \frac{\dot{Q}_{reac}}{\rho_s \cdot (1-\epsilon) \cdot c_s} - \frac{4 \cdot h_{out} \cdot \left(T_{cat}^i - T_{amb}\right)}{D_{cat} \cdot \rho_s \cdot (1-\epsilon) \cdot c_s} \end{aligned} \tag{14}$$

As for the oxygen storage model, the FDM procedure leads to:

$$\frac{d\phi^i}{dt} = \frac{1}{OSC} \cdot \left(2 \cdot R_1^i - R_2^i\right) \tag{15}$$

$$\begin{aligned} R_1^i &= k_1^f \cdot [Ce_2O_3]^{i^2} \cdot [O_2]^i - k_1^b \cdot [Ce_2O_4]^{i^2} \cdot c_0 \\ R_2^i &= k_2^f \cdot [Ce_2O_4]^i \cdot [CO]^i - k_2^b \cdot [Ce_2O_3]^i \cdot [CO_2]^i \end{aligned} \tag{16}$$

whereas, gas species concentration dynamics (8), are discretized as follows:

$$\begin{aligned} [O_2]^i &= [O_2]^{i-1} - R_1^i \cdot \frac{c_0 \cdot M_{exh} \cdot A_{cs} \cdot \Delta z}{\dot{m}_{exh}} \\ [CO]^i &= [CO]^{i-1} - R_2^i \cdot \frac{c_0 \cdot M_{exh} \cdot A_{cs} \cdot \Delta z}{\dot{m}_{exh}} \\ [CO_2]^i &= [CO_2]^{i-1} + R_2^i \cdot \frac{c_0 \cdot M_{exh} \cdot A_{cs} \cdot \Delta z}{\dot{m}_{exh}} \end{aligned} \tag{17}$$

In [13], a sensitivity analysis of the overall model performance with respect to the number of discretization cells resulted in an optimal choice of five cells for the thermal model and three cells for the oxygen storage model.

IV. Dual Extended Kalman Filter

The goal of the d-EKF observer is to estimate ϕ and OSC during vehicle operation. An observer is needed as both these quantities cannot be directly measured and instantaneous information about their values is crucial to both optimize TWC efficiency and enable onboard diagnostics. The proposed d-EKF has four state variables: the first three states are from the discretization of (15) to predict SOX; the fourth state variable represents the slowly varying (due to aging) oxygen storage capacity, OSC. The predicted output is the normalized air/fuel ratio, λ_{mid} downstream the catalytic converter. Inputs to the model observer are the air/fuel ratio lambda upstream the catalyst, λ_{pre}, the exhaust mass flow rate, $\dot{m}_{exh}$, and predicted catalyst temperature from the physics-based thermal model, T_{cat}. The states, input and output vectors are shown below:

$$x = \begin{vmatrix} \phi_1 \\ \phi_2 \\ \phi_3 \\ OSC \end{vmatrix} \quad u = \begin{vmatrix} \dot{m}_{exh} \\ T_{cat} \\ \lambda_{pre} \end{vmatrix} \quad y = \lambda_{mid} \tag{18}$$

The d-EKF control scheme is shown in Figure 3. For

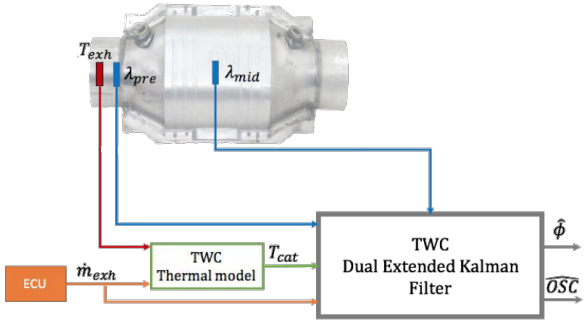

Fig. 3: Control scheme of the d-EKF designed for TWC.

the purpose of designing the d-EKF, the TWC nonlinear dynamics obtained from FDM can be presented in state-space form:

$$\begin{aligned} \dot{x}(t) &= f\left(x(t), u(t)\right) + v(t), & v(t) &\sim \mathcal{N}(0, Q) \\ y(t) &= g\left(x(t), u(t)\right) + w(t), & w(t) &\sim \mathcal{N}(0, R) \end{aligned} \tag{19}$$

where $v(t)$ and $w(t)$ are uncorrelated stochastic noises which take into account model and output discrepancies. The model

uncertainty $v(t)$ is modeled as a Gaussian zero mean white noise with a semi-definitive positive covariance square matrix $Q \in \mathbb{R}^{4\times4}$:

$$Q = diag\begin{pmatrix} Q_1 & \dots & Q_4 \end{pmatrix} \tag{20}$$

The output uncertainty $w(t)$ is also a Gaussian zero mean white noise with a strictly positive variance, $R \in \mathbb{R}^{1\times1}$ [19]. The nonlinear equations describing the SOX dynamics are obtained from (11), whereas the OSC aging parameter rate of change is assumed to be zero (slow variable). The predicted air/fuel ratio λ_{mid} is evaluated from the gas species concentrations from (12). Model and output nonlinear equations become:

$$\begin{aligned}
\dot{x}_1(t) &= \frac{d\phi_1}{dt} = f_1\left(x(t),u(t)\right) = \frac{1}{x_4}\cdot\left(2\cdot R_1^1 - R_2^1\right) + v_1\\
\dot{x}_2(t) &= \frac{d\phi_2}{dt} = f_2\left(x(t),u(t)\right) = \frac{1}{x_4}\cdot\left(2\cdot R_1^2 - R_2^2\right) + v_2\\
\dot{x}_3(t) &= \frac{d\phi_3}{dt} = f_3\left(x(t),u(t)\right) = \frac{1}{x_4}\cdot\left(2\cdot R_1^3 - R_2^3\right) + v_3\\
\dot{x}_4(t) &= \frac{dOSC}{dt} = f_4\left(x(t),u(t)\right) = 0 + v_4\\
y(t) &= \lambda_{mid} = g\left(x(t),u(t)\right) = \frac{2\cdot\left([O_2]+[CO_2]\right)+[CO]}{2\cdot\left([CO]+[CO_2]\right)} + w
\end{aligned} \tag{21}$$

Kalman filter dynamic equations are defined in the discrete time domain as follows:

$$\begin{aligned}
\hat{x}(k+1|k) &= f\left(\hat{x}(k|k-1),u(k)\right)\\
&\quad + K(k)\cdot\left(y(k) - g\left(\hat{x}(k|k-1),u(k)\right)\right)\\
\hat{y}(k) &= g\left(\hat{x}(k|k-1),u(k)\right)
\end{aligned} \tag{22}$$

where $K(k)$ is the Kalman filter gain, [19], which is updated as follows:

$$K(k) = \hat{A}(k)\tilde{P}(k|k-1)\hat{C}(k)^T\left(\hat{C}(k)\tilde{P}(k|k-1)\hat{C}^T(k) + R\right)^{-1} \tag{23}$$

$\tilde{P}(k|k-1)$ is the solution of the Algebraic Riccati Equation which minimizes the estimate covariance error $\tilde{P}(k|k-1) = E\left[\left(x(k)-\hat{x}(k|k-1)\right)\cdot\left(x(k)-\hat{x}(k|k-1)\right)^T\right]$. $\hat{A}$ and $\hat{C}$ are the matrices of the linearized system calculated at each time step based on the predicted states $\hat{x}(k|k-1)$ and input $u(k)$, [20], [21]:

$$\hat{A}(k) = \left.\frac{\partial f(x,u)}{\partial x}\right|_{\hat{x}(k|k-1),u(k)} \qquad \hat{C}(k) = \left.\frac{\partial h(x,u)}{\partial x}\right|_{\hat{x}(k|k-1),u(k)} \tag{24}$$

V. Results

The d-EKF has been tested and calibrated under real driving conditions (Federal Test Procedure - FTP)[1]. Figure 4 shows the observer performance in terms of estimated ϕ. Convergence is obtained after 700 seconds thanks to the convergence of the aging parameter OSC to its actual value. In fact, as discussed in Section III, the prediction of the output λ_{mid} and SOX is dependent on the OSC value. Furthermore, the predicted output $\lambda_{mid_{Sim}}$ improves as the estimated OSC value converges to the actual value.

The robustness of the d-EKF is tested across different initial conditions of OSC. As shown in Figure 5, after an initial transient, all the estimates converge to the nominal value. Practically, convergence of OSC is reached within the first 700 seconds, despite the initial condition the filter was initialized to. The only instance where longer time to converge is requested (around 1000 seconds) is when the initialization sets $OSC_{normalized} > 1$ [2]. This condition is used to test convergence robustness of the observer. Figure 6 shows the OSC estimation convergence as a function of the covariance Q_4. Large values of Q_4 leads to a quick convergence at the price of more oscillatory behavior at steady state. On the other hand, a smaller value of the tuning parameter leads to a smoother trajectory, but much slower response. As OSC is a slow varying dynamic, a slow convergence is acceptable. Therefore, for the final tuning in this study we used $Q_4 = 0.00002$, which corresponds to a convergence time of 1000 seconds.

VI. Conclusion

In this paper, a d-EKF is developed to estimate the oxygen storage dynamics and oxygen storage capacity of a TWC. A nonlinear control-oriented model is utilized for the observer design, obtained through FDM of PDE model from [13]. The developed observer estimates the oxygen storage, SOX, and capacity, OSC, using wide range oxygen sensors located upstream and downstream the converter and its performance is evaluated under a standard real driving scenario, and against different initial conditions of operation.

Acknowledgment

The authors greatly acknowledge the financial support from FCA US LLC (Auburn Hills, MI 48326 USA).

References

[1] "Epa." `http://yosemite.epa.gov/opa/admpress.nsf`.

[2] M. Santillo, S. Magner, M. Uhrich, and M. Jankovic, "Towards ecu-executable control-oriented models of a three-way catalytic converter," *Proceedings of the ASME DSCC2015-9653*, 2015.

[3] S. B. Kang, S. J. Han, I. S. Nam, B. K. Cho, C. H. Kim, and S. H. Oh, "Detailed reaction kinetics for double-layered Pd/Rh bimetallic TWC monolith catalyst," *Progress in energy and combustion science*, 2005.

[4] E. Shafai, C. Roduner, and H. P. Geering, "Indirect adaptive control of a three-way catalyst," *SAE Technical Paper 961038*, 1996.

[5] C. Ngo, D. Koenig, O. Sename, and H. Béchart, "A reduced model of three ways catalyst converter and stored oxygen rate estimation using switched observer," *12th biannual European Control Conference (ECC 2013)*, 2013.

[6] K. R. Muske and J. C. P. Jones, "Estimating the oxygen storage level of a three-way automotive catalyst," *Proceedings of American Control Conference, 2004*, 2004.

[7] P. Kumar, I. Makki, and D. Filev, "A non-intrusive three-way catalyst diagnostics monitor based on support vector machines," *2014 IEEE International Conference on Systems, Man, and Cybernetics*, 2014.

[8] T. S. Auckenthaler, C. H. Onder, and H. P. Geering, "Online estimation of the oxygen storage level of a three-way catalyst," *SAE Technical Paper 2004-01-0525*, 2004.

[9] T. Utz, C. Fleck, J. Frauhammer, D. Seiler-Thull, and A. Kugi, "Extended Kalman filter and adaptive backstepping for mean temperature control of a three-way catalytic converter," *International Journal of Robust and Nonlinear Control*, 2014.

[1] For confidentiality reasons, the validation plots for the OSC estimation have been normalized with respect to the maximum OSC value corresponding to the oxygen storage capacity of a fresh catalyst.

[2] Simulation results reported in this paper were obtained assuming an initial OSC value greater than the fresh catalyst value of 1 to account for wrong OSC initialization.

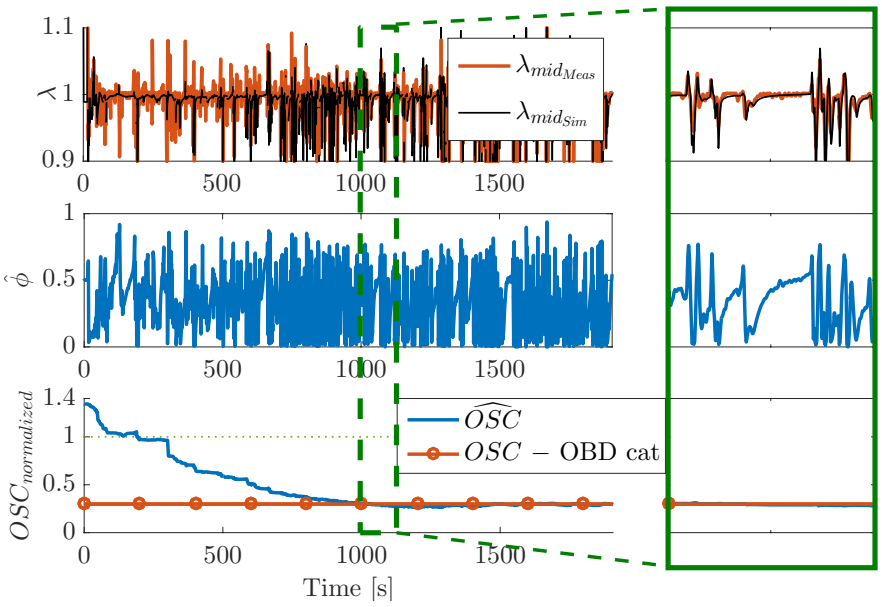

Fig. 4: Simulation results of the estimated output (compared to λ_{mid} measured), $\hat{\phi}$ is the average value of SOX evaluated with the three spatial discretization cells and $\widehat{OSC}$ is the estimate of oxygen storage capacity (normalized with respect to the OSC of a fresh catalyst) and a zoom-in over the time window between 1000 and 1100 seconds.

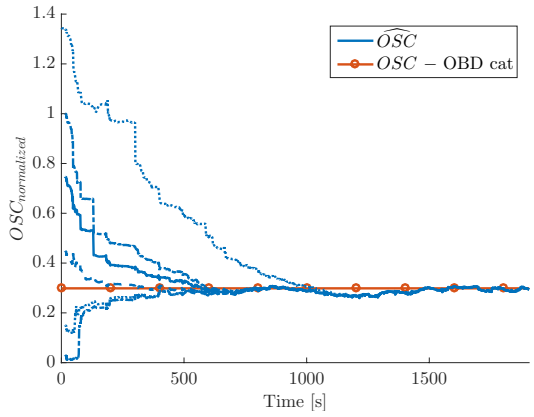

Fig. 5: Estimation of OSC - normalized with respect to OSC value from fresh catalyst - for different initialization values of the estimator.

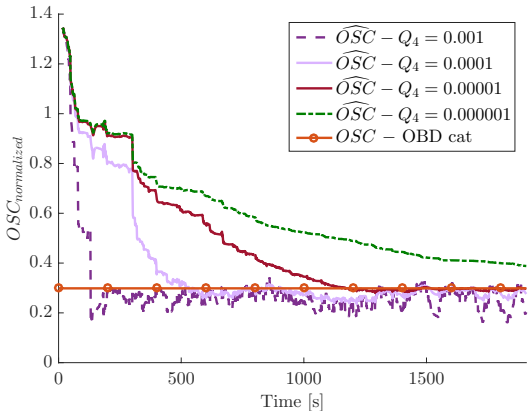

Fig. 6: Estimation of OSC - normalized with respect to OSC value from fresh catalyst - for different values of the variance Q_4.

[10] S. Sabatini, I. Kil, J. Dekar, T. Hamilton, J. Wuttke, M. Smith, M. A. Hoffman, and S. Onori, "A new semi-empirical temperature model for the three way catalytic converter," *IFAC Workshop on Engine and Powertrain Control, Simulation and Modeling*, 2015.

[11] S. Sabatini, I. Kil, J. Dekar, T. Hamilton, J. Wuttke, M. Smith, M. A. Hoffman, Z. Filipi, and S. Onori, "Characterization of aging effect on three way catalyst oxygen storage dynamics," *SAE Technical Paper 2016-01-0971*, 2016.

[12] "Science china chemistry." `http://chem.scichina.com:8081/sciBe/EN/volumn/volumn_6983.shtml`.

[13] S. Sabatini, S. Gelmini, M. A. Hoffman, and S. Onori, "Design and experimental validation of a physics-based oxygen storage - thermal model for three way catalyst including aging," *Under review*, 2016.

[14] T. Shamim, H. Shen, S. Sengupta, S. Son, and A. Adamczyk, "A comprehensive model to predict three-way catalytic converter performance," *Journal of engineering for gas turbines and power*, 2002.

[15] G. Montenegro and A. Onorati, "1D thermo-fluid dynamic modeling of reacting flows inside three-way catalytic converters," *SAE Technical Paper 2009-01-1510*, 2009.

[16] P. Kiwitz, C. Onder, and L. Guzzella, "Control-oriented modeling of a three-way catalytic converter with observation of the relative oxygen level profile," *Journal of Process Control*, 2012.

[17] C. Depcik and D. Assanis, "One-dimensional automotive catalyst modeling," *Progress in energy and combustion science*, 2005.

[18] R. J. LeVeque, *Finite difference methods for ordinary and partial differential equations: steady-state and time-dependent problems*. Siam, 2007.

[19] L. Ljung, *System identification*. Springer, 1998.

[20] M. S. Grewal, *Kalman filtering*. Springer, 2011.

[21] L. Magni and R. Scattolini, *Advanced and multivariable control*. Pitagora, 2014.